Princeton Plasma Physics Laboratory

PPPL-4141
PPPL-4141

Long Pulse High Performance Plasma Scenario Development for the National Spherical Torus Experiment

C.E. Kessel, R.E. Bell, M.G. Bell, D.A. Gates, R.W. Harvey, S.M. Kaye, B.P. LeBlanc, T.K. Mau, J.E. Menard, C.K. Phillips, P.M. Ryan, S.A. Sabbagh, E.J. Synakowski, G. Taylor, R. Wilson, and the NSTX Research Team

January 2006

PPPL PRINCETON PLASMA PHYSICS LABORATORY

Prepared for the U.S. Department of Energy under Contract DE-AC02-76CH03073.

Princeton Plasma Physics Laboratory
Report Disclaimers

Full Legal Disclaimer

Trademark Disclaimer

PPPL Report Availability

Princeton Plasma Physics Laboratory

This report is posted on the U.S. Department of Energy's Princeton Plasma Physics Laboratory Publications and Reports web site in Fiscal Year 2006.

The home page for PPPL Reports and Publications is:

http://www.pppl.gov/pub_report/

Office of Scientific and Technical Information (OSTI):

Available electronically at: http://www.osti.gov/bridge.

Available for a processing fee to U.S. Department of Energy and its contractors, in paper from:

U.S. Department of Energy
Office of Scientific and Technical Information
P.O. Box 62
Oak Ridge, TN 37831-0062

Telephone: (865) 576-8401

Fax: (865) 576-5728

E-mail: reports@adonis.osti.gov

Long pulse high performance plasma scenario development for the National Spherical Torus Experiment

C. E. Kessel, R. E. Bell, M. G. Bell, D. A. Gates, R. W. Harvey[1], S. M. Kaye, B. P. LeBlanc, T. K. Mau[2], J. E. Menard, C. K. Phillips, P. M. Ryan[3], S. A. Sabbagh[4], E. J. Synakowski, G. Taylor, R. Wilson and the NSTX Research Team
Princeton Plasma Physics Laboratory, Princeton, NJ, USA
[1]CompX, Del Mar, CA, USA
[2]University of California, San Diego, CA, USA
[3]Oak Ridge National Laboratory, Oak Ridge, TN, USA
[4]Columbia University, New York, NY USA
ckessel@pppl.gov

Abstract.
The National Spherical Torus Experiment (NSTX) [Ono, M., et al., Nucl. Fusion, **44**, (2004), 452.] is targeting long pulse high performance, non-inductive sustained operations at low aspect ratio, and the demonstration of non-solenoidal startup and current rampup. The modeling of these plasmas provides a framework for experimental planning and identifies the tools to access these regimes. Simulations based on NBI (Neutral Beam Injection)-heated plasmas are made to understand the impact of various modifications and identify the requirements for 1) high elongation and triangularity, 2) density control to optimize the current drive, 3) plasma rotation and/or feedback stabilization to operate above the no-wall β limit, and 4) Electron Bernstein Waves (EBW) for off-axis heating/current drive (H/CD). Integrated scenarios are constructed to provide the transport evolution and H/CD source modeling, supported by rf and stability analyses. Important factors include the energy confinement, Z_{eff}, early heating/H-mode, broadening of the NBI-driven current profile, and maintaining q(0) and q_{min}>1.0. Simulations show that non-inductive sustained plasmas can be reached at I_P=800 kA, B_T=0.5 T, κ≈2.5, $\beta_N \leq 5$, β≤15%, f_{NI}=92%, and q(0)>1.0 with NBI H/CD, density control, and similar global energy confinement to experiments. The non-inductive sustained high β plasmas can be reached at I_P=1.0 MA, B_T=0.35 T, κ≈2.5, $\beta_N \leq 9$, β≤43%, f_{NI}=100%, and q(0)>1.5 with NBI H/CD and 3.0

MW of EBW H/CD, density control, and 25% higher global energy confinement than experiments. A scenario for non-solenoidal plasma current rampup is developed using High Harmonic Fast Wave (HHFW) H/CD in the early low I_P and low T_e phase, followed by NBI H/CD to continue the current ramp, reaching a maximum of 480 kA after 3.4 s.

I. Introduction

The National Spherical Torus Experiment (NSTX) will provide the physics basis to assess the fusion potential of the spherical torus concept[1]. In order to do this NSTX is targeting four specific goals; operation with 100% of the plasma current supplied non-inductively for more than a current redistribution time (τ_{CR}), operation of high β ($\beta = 2\mu_o\langle p\rangle/B_{To}^2 \approx$ 30-40%, $\beta_N = \beta/(I_P/aB_T) > \beta_N^{\text{no-wall}}$) and high energy confinement ($H_{98(y,2)} > 1.2$, global energy confinement multiplier [2]) plasmas for several energy confinement times, demonstration of non-solenoidal breakdown/startup and plasma current rampup, and the integration goal of operating high β plasmas with high confinement and 100% of the plasma current supplied non-inductively for several current redistribution times. Integrated simulations are performed to determine the requirements for NSTX to meet these goals by reconstructing experimental discharges and projecting to these advanced plasma configurations. In addition, where little experimental information exists, reasonable assumptions and theoretical models are applied until such information is available. The use of simulations on NSTX is expected to evolve as physics models are developed, experimental results are available, and integrated discharge simulation tools improve.

II. Computational Approach

The Tokamak Simulation Code (TSC)[3] is used for the predictive time-dependent transport simulations. This code solves the axisymmetric 2-dimensional MHD-Maxwell's equations on a rectangular grid in (R,Z) space. 1-dimensional flux surface averaged transport equations are solved for energy, particles, and current density utilizing pre-defined transport coefficients (from theoretical models or experimental data). The plasma is free-boundary so that surrounding conducting structures and poloidal field coils are included, allowing feedback systems to be

incorporated. The code also has numerous peripheral physics models for bootstrap current, sawtooth evolution, ripple losses, etc.

TRANSP[4] is used in the interpretive mode, where it receives equilibrium reconstructions from the experiments, ion and electron temperature profile data, electron density profile data, Z_{eff} profile data, plasma rotation profile data, and solves flux conservation equations governing flux surface averaged 1-dimensional transport for energy, particles, current density, and momentum. The current density is typically not evolved, but constrained by the equilibrium reconstructions provided by EFIT. The recent introduction of the Motional Stark Effect (MSE) diagnostic on NSTX gives considerably greater confidence in this constraint. The neutral beam injection (NBI) properties in the plasma are calculated with NUBEAM[5,6], a Monte Carlo orbit following algorithm. TRANSP contains several peripheral physics models, fast particle physics, and neutral particle effects.

The CURRAY[7] code is a 3-dimensional ray-tracing calculation for rf waves in the frequency range from ion cyclotron to lower hybrid. It is used here to examine High Harmonic Fast Wave (HHFW) heating and current drive. The ray equations are based on the cold dispersion relation, with relevant thermal electron corrections. Absorption mechanisms include electron Landau and transit time magnetic pumping (TTMP), ion cyclotron resonances at the fundamental and higher harmonics for thermal and slowing down distributions. At present, beam energetic ion absorption is modeled by an equivalent Maxwellian distribution with a characteristic temperature and anisotropy. The GENRAY and CQL3D[8,9] codes are used to establish the Electron Bernstein Wave (EBW) deposition and current drive. GENRAY is a ray-tracing calculation based on the Stix hot plasma, non-relativisitic dispersion relation. CQL3D is a relativistic Fokker-Planck calculation which solves for the bounce-averaged, 2-dimensional (momentum space) electron distribution function. The wave absorption, although calculated in GENRAY, is recalculated after coupling the ray information to the Fokker-Planck calculation, including relativistic effects and is consistent with the resulting non-Maxwellian distributions.

Some ideal MHD stability analysis will be given for selected scenario flattop plasmas. These are analyzed using an equilibrium description directly from TSC, which is read into the fixed boundary flux coordinate equilibrium code JSOLVER[10]. JSOLVER recalculates the equilibrium with high resolution for stability analysis. High-n ballooning stability is calculated

with BALMSC[11], and n=1 and 2 external kink stability is assessed with PEST2[12] or DCON[13]. The wall models used in the low-n stability analysis are shown in Fig. 1, one which is aligned with the actual conducting structure locations in NSTX, and the other intended to be more conservative to account for the nonaxisymmetries present in the NSTX structures. Work to develop an axisymmetric equivalent model of the actual 3-dimensional structures using VALEN[14] is ongoing and will improve the identification of stability boundaries.

III. Experimental Progress on Long Pulse Discharges in NSTX

Substantial progress has been made in producing long pulse discharges in NSTX, and this will be briefly discussed by using a single discharge from the last three run campaigns; 109070 (2002), 112546 (2004), and 116313 (2005). The pulse lengths for these discharges are 0.55 s, 1.05 s, and 1.50 s, respectively, the last of which reached the toroidal field coil I^2t heating limit. In the 2002 run period, another discharge actually lasted longer than 109070, with similar parameters, out to 0.9 s, but had data acquisition problems and was not analized. Discharge 109070 had I_P = 800 kA and B_T = 0.5 T, discharge 112546 had I_P = 800 kA and B_T = 0.5 T, and discharge 116313 had I_P = 750 kA and B_T = 0.45 T. Shown in Fig. 2 are the plasma currents, neutral beam injection (NBI) heating trajectories, plasma elongations, and internal self-inductances. The two later discharges, 112546 and 116313 utilize an early heating and H-mode transition. Here 2 of the 3 NB sources are injected while the plasma current is being ramped up, and the 3rd source is injected near the end of the plasma current ramp. A flat spot is made in the plasma current ramp at about the time that the 2 NB sources are injected inducing an H-mode with the plasma current at roughly 450-500 kA. The earlier discharge 109070 injected only 1 NB source during the current ramp, and 2 after the current ramp was completed. For this case the H-mode does not occur until the plasma current is at its full value of 800 kA. The early onset of the H-mode causes the plasma to consume significantly less volt-seconds in the early phase of the discharge, creating longer flattop capability from the solenoid. From Fig. 2, the discharge pulse length has been extended progressively each run campaign and the plasma elongation is routinely above 2.25 for the recent discharges. One of the more interesting results from the 2005 run period is the sustainment of the current profile, shown as li(1), for about 3 current redistribution times, versus a constantly rising li(1) value for the 2004 run period. The low value of li(1), about 0.6, indicates a broad current profile which is attributed to the bootstrap current, since the NBI

current drive is peaked on axis, and as will be discussed later the bootstrap fraction reached over 50%.

Shown in Fig. 3 are the β_N, peak density, peak electron temperature, and surface voltage as a function of time for the 3 discharges. The discharge 109070 has a much higher electron temperature than the two discharges with an early H-mode, which results in a very low surface voltage. This higher temperature can not be attributed to the slightly lower density, and this plasma likely obtained an enhanced confinement regime. All the discharges have a constantly rising density, so that a longer pulse length ultimately ends up at a higher density. In fact, 116313 reaches just over 90% of the Greenwald density ($n_{Gr} = I_P/\pi a^2$). All 3 discharges reach approximately $\beta_N = 6$, with 109070 disrupting, while the two more recent discharges have the onset of MHD that reduces their stored energy. Analysis indicated that 109070 may have disrupted from reaching the with-wall n=1 external kink limit[15]. Discharge 112546 is terminated after the NBI was shutoff at 1.0 s. Discharge 116313 continues for 0.5 s after a drop in the stored energy making β_N drop from 6.0 to 4.5, with the discharge ending from a preprogrammed shutdown of the toroidal field coil. The most striking differences between these discharges is the confinement regime between 109070 and the recent discharges 112546 and 116313, and the different current profile (li) evolutions between 112546 and 116313. Analysis of these differences is intended to provide the basis for discharge optimization in the future.

IV. Simulations of 100% Non-inductive Sustained Plasmas for $\tau_{flat} > \tau_{CR}$ Based on Discharge 109070

Initial discharge simulations to produce 100% non-inductive current plasmas were based on the discharge 109070. The discharge 109070, which was NBI heated, is used as the basis for these simulations because it achieved 50% non-inductive current fraction, a β_N exceeding 6.0, and an $H_{98(y,2)}$ value of 1.25, with an I_P and β flattop time of about one current redistribution time. The factor $H_{98(y,2)}$ represents a multiplier on the IPB98(y,2) global energy confinement scaling developed in ref[2]. For this discharge I_P = 800 kA, B_T = 0.5 T, R = 0.88 m, a = 0.59 m, elongation κ = 2.05, triangularity $\langle\delta\rangle$ = 0.45, bootstrap current I_{BS} = 240 kA, and neutral beam driven current I_{NB} = 160 kA, all evaluated at 450 ms. A benchmark calculation in TSC to reproduce the discharge behavior was performed by taking the plasma H-mode properties at 0.45

s, prior to any MHD in the discharge, and applying it throughout the H-mode phase, from 0.2 to 0.55 s. The thermal diffusivities, density profile, Z_{eff} profile, NB heating profile, fast ion density and pressure, and NB driven current were obtained from TRANSP analysis of the discharge. Prior to 200 ms a theoretical L-mode model is used for the thermal diffusivities for electrons and ions prior to the H-mode transition, both in the simulations of the experiments and the projections. Shown in Fig. 4 are the peak electron and ion temperatures as a function of time in the discharge and the TSC simulation, showing reasonable agreement, although not reproducing the L to H transition phase well, as would be expected. Also shown are the profiles from the simulation at 0.45 s, showing the safety factor, thermal diffusivities, temperature profiles, and density profile. Several other parameters were matched such as li, loop voltage, plasma shape, and stored energy. In order to project this discharge to new plasma parameters, the thermal diffusivities are spatially fixed and scaled by the IPB98(y,2) scaling, the density and Z_{eff} and their profiles are prescribed, and TRANSP NBI characteristics listed above are used.

The simulation of 109070 demonstrated that the constantly rising density was suppressing the NBI driven current, and that the on-axis safety factor reached the vicinity of 1.0 around the disruption time of 0.55 s. In addition, the bootstrap current was unaffected by the density rise. In order to increase the non-inductive current fraction we maintain the toroidal field at the 109070 value of 0.5 T, to help keep the safety factor above 1.0. This toroidal field value has a maximum pulse length of 1.5 s. The plasma current is kept at 800 kA, and the absorbed NBI power is 5.5 MW. The plasma elongation was increased from 2.0 to 2.5 to enhance the bootstrap current fraction, the density was reduced from 0.5 to 0.3×10^{20} /m^3 and assumed to be controlled to elevate the NBI driven current, and more NBI power was injected earlier to induce an early H-mode. The NBI source injection for 109070 was the 1st source at 0.10 s, the 2nd source at 0.20 s, and the 3rd source at 0.25 s. For the early heating scenario 2 sources are injected at 0.10 s, and the 3rd source is injected at 0.20 s. The NBI power absorption in the plasma takes account of the weaker confinement of the NB fast ions at lower plasma currents, which reduces the absorbed power, and can have a significant effect on the safety factor evolution, as will be discussed later. Shown in Fig. 5 are the plasma current and central safety factor for 109070 (pink) and the projected discharge (blue). For the projected discharge the non-inductive current fraction reaches 92%, and the central safety factor reaches 1.0 at 1.5 s, which is the maximum pulse available. The central safety factor drops during the discharge because the NBI driven current is

centrally peaked, but the early heating and H-mode transition raises the safety factor early in the discharge so it takes significantly longer to reach 1.0 compared to 109070. The predicted bootstrap and NBI currents are each 355 kA, β_N reaches 4.7 and the $H_{98(y,2)}$ factor is 1.23. Fig. 5 shows the parallel current densities for 109070 (pink) and the projected discharge (blue), which show that 109070 has considerable inductive current in its profile (the difference between the total and the NBCD and bootstrap components), while the projected case is aligned with the non-inductive current sources. The projected case also has a higher on-axis current density than 109070 since it has relaxed during its longer pulse length, while 109070 has not relaxed. This projected discharge is one example of several variations of the three critical features (and energy confinement) cited above that were examined to produce 100% non-inductive plasmas.

V. Simulations of 100% Non-inductive Sustained Plasmas for $\tau_{flat} > \tau_{CR}$ Based on Discharge 116313

The recent discharge 116313 (2005) achieved a bootstrap current fraction approaching 50%, and a total non-inductive current fraction of over 70%. In addition, β_N was sustained at 5.5-6.0 for about 2 τ_{CR}, the internal self-inductance was maintained for 3 τ_{CR}, and the plasma current was in flattop for about 5 τ_{CR}. For this discharge I_P = 750 kA, B_T = 0.45 T, R = 0.88 m, a = 0.59 m, elongation κ = 2.3, triangularity $\langle\delta\rangle$ = 0.65, bootstrap current I_{BS} = 400 kA, and neutral beam driven current I_{NB} = 80 kA, all evaluated at 980 ms. The energy confinement in this discharge was lower than that for the discharge 109070, indicated by the lower electron and ion temperatures between 0.2 and 0.5 s, while the densities and injected powers were similar. A benchmark calculation was done using TSC to reproduce the discharge. In this case a slightly different procedure was used than in the case of 109070. The experimental density profiles, electron and ion temperature profiles are input to TSC, and the NBI power deposition profiles are obtained from a TRANSP run of the discharge using EFIT reconstructions with the MSE including the E_r correction from plasma rotation. An algorithm is used in the TSC code allowing it to determine the thermal diffusivities for ions and electrons while still solving a predictive simulation[16]. The plasma density is forced to follow the experimental data. The free-boundary evolution of the plasma is provided by the experimental poloidal field coil currents, and feedback control systems on the plasma radial and vertical position, and plasma current. Shown in Fig. 6 are the peak electron and ion temperatures from the TSC simulation and from

the data, indicating reasonable agreement. Also shown is the evolution of the density, indicating that there is substantial density profile peaking, which is known to enhance the bootstrap current. Various plasma profiles are also shown in Fig.6, demonstrating that the electron and ion temperature profiles are quite different from those of 109070, in addition to the density profile. In Fig. 7 the contributions to the plasma current are given, showing that the bootstrap current is reaching 400 kA, more than 50% of the plasma current, while the NBCD is suppressed and only reaches about 80 kA between 0.5 and 1.0 s. The total non-inductive current fraction is exceeding 70%. Also shown is the time evolution of the safety factor on axis from the TSC simulation and the EFIT reconstructions with MSE constraint. The agreement is reasonable, although the phase between 0.2 and 0.4 s requires further improvement. Regardless, both trajectories indicate that the safety factor did not reach 1.0. However, the MHD spectrum (Mirnov measurements) shows that a low frequency n=1 mode emerges at about 1.05 s, and persists to the end of the discharge. The plasma stored energy drops during this phase bringing β_N from 6.0 to 4.5. It should be noted that once a low-n MHD mode is present in the plasma, an axisymmetric simulation like that with the TSC will not reproduce the safety factor since it doesn't contain the physics models for this. However, it is reproducing the loss in stored energy as a result of this MHD, which results in the safety factor (and other parameters) following a trajectory that is inconsistent with the experiment.

It is of interest to understand the difference between the two discharges 109070 (2002) and 116313 (2005), since they have strongly different energy confinement, which may be the result of different safety factor profile evolutions. In fact, for 109070 at 0.45 s, the peak electron temperature is nearly twice, and the peak ion temperature is three times the peak temperatures for 116313. It is found in the simulations that the H-mode transition and the NBI power absorption at that time plays a role in the formation of reversed shear in the safety factor profile. The discharge 109070 undergoes an H-mode transition at 0.2 s, when the plasma current is at its maximum of 800 kA, and the 2nd NB source in injected. The 3rd NB source is injected at 0.25 s. The simulations indicate that at 0.2 s the safety factor profile is monotonic, but after the transition and heating, it becomes reversed, and this reversal persists during the discharge, at least until after 0.45 s. In the more recent discharge 116313, the early heating and H-mode technique is being used. In this case the H-mode transition occurs at about 0.085 s during the plasma current ramp, with the plasma current at 450-500 kA. At this time 2 NB sources are

injected in rapid succession, but at this lower current, the NBI power absorbed by the plasma is low due to losses of the fast ions. Although this heating seems to mildly amplify the reversed shear in the safety factor already present from the I_P ramp, it is not adequate to maintain it. The shear reversal is lost by 0.15 s, which is before the plasma current has reached its maximum value of 750 kA. The safety factor profiles from the simulations are shown in Fig. 8. The safety factor profiles from 116313 determined from EFIT reconstructions with the MSE constraint (including Er corrections) confirms this evolution in the safety factor profile found in the TSC simulation. The MSE diagnostic was not available during the 2002 run campaign. This difference in the early formation leads to higher energy confinement ($H_{98(y,2)}$ = 1.25 versus 1.1) in 109070 than 116313, however, the later discharge has better sustainment properties. Future simulations will examine how changes in the heating and plasma current trajectories can produce profile evolutions that fall between these two cases, in order to balance the confinement and MHD stability properties.

Since the most recent long pulse experiments have demonstrated two of the features highlighted by simulations to achieve 100% non-inductive current, high κ and early heating/H-mode, it is useful to examine the impact of density control on these discharges. In these simulations the plasma density profile is prescribed by an analytic profile, and its magnitude is specified. The thermal diffusivities are taken from the TSC reproduction simulation of discharge 116313 at 4 time slices (t = 0.10, 0.25, 0.50, and 0.75 s) and interpolated/extrapolated for other time points. These are spatially fixed and then scaled by the IPB98(y,2) global energy confinement scaling to account for changes in global parameters. The NBI characteristics are taken from TRANSP. Shown in Fig. 9 are the central safety factors as a function of time for 4 cases, two with peaked density profiles, and two with broad density profiles, and each of these with higher and lower energy confinement. The plasma density is reduced to 0.42 x 10^{20} /m^3, from the reference value of 0.92 x 10^{20} /m^3 and held fixed in the flattop. This results in peak electron temperatures of 1.05-1.5 keV. The point at which the central safety factor reaches 1.0 is designated by the circles. The trajectories indicate that in order to keep the safety factor above 1.0, higher confinement is beneficial since it increases the bootstrap current, although it also tends to increase the NB driven current as well. The peaked density cases are also doing better in this regard. The $n(0)/\langle n\rangle$ = 1.7 and $H_{98(y,2)}$ = 1.2 case yields a non-inductive current fraction of 88%, while the $H_{98(y,2)}$ = 1.1 yields 78%. The $n(0)/\langle n\rangle$ = 1.15 and $H_{98(y,2)}$ = 1.15 case yields a non-

inductive current fraction of 73%, while the $H_{98(y,2)} = 0.93$ yields 53%. Examining the highest non-inductive current case with $n(0)/\langle n \rangle = 1.7$ and $H_{98(y,2)} = 1.2$, Fig. 9 shows the parallel current densities for the reference discharge 116313 and the projected discharge. The NBCD is increased from 80 kA to 350 kA, and the bootstrap current is reduced from 400 kA to 275 kA. The drop in the bootstrap current is due to an overall drop in the plasma stored energy when lowering the density. The NB current density is much higher in the core and is peaking the total current density over that from the reference discharge. Overall, these simulations, based on the energy confinement of discharge 116313, indicate that the lower density is beneficial for raising the NB component to the non-inductive current, although this must be balanced with its tendency to drive the central safety factor below one. Higher densities will be pursued to optimize this tradeoff.

VI. Simulations of 100% Non-inductive Sustained High β Plasmas for $\tau_{flat} >> \tau_{CR}$ Based on Discharge 109070

The integration goal for NSTX is to combine the 100% non-inductive sustainment and high β for times much longer than a current redistribution time, so as to produce a plasma configuration that can be projected to steady state high fusion performance. The discharge 109070 (2002) is used as the reference for projecting to this plasma regime. Identified in the 100% non-inductive plasma projections were three critical features for reaching that goal; higher κ, early heating/H-mode transition, and density control. These are also required for these high β cases, but we will need to add higher energy confinement, Electron Bernstein Wave (EBW) off-axis current drive, and some degree of broadening of the NB driven current to reach the highest β's. The toroidal field is lowered to 0.35 T, the EBW is assumed to provide 3 MW of power to the plasma, and the NB energy is increased to provide 6.75 MW. The decrease in the toroidal field and any increase in plasma current are balanced against getting the various CD sources (including bootstrap) to provide the entire current and avoid the safety factor getting too low. The lower B_T allows the available flattop time to increase to 3.5 s.

Due to the low toroidal field typical of spherical tori, the plasma is overdense, with $\omega_{pe}^2/\omega_{ce}^2 >> 1$, and conventional electron cyclotron waves can not propagate. EBWs can propagate in these plasmas and are strongly absorbed at the cyclotron resonances. These EBWs can be

produced by mode conversion of electron cyclotron waves in the vicinity of the upper hybrid layer, which is near the plasma surface on the low field side for ST parameters. Shown in Fig. 10 are the results of analysis with the GENRAY/CQL3D codes to determine the current drive deposition of the EBWs in NSTX projected plasmas at $\beta = 20$ and 40%, and at 14 and 28 GHz. The calculations show that the current is driven off-axis in a similar location over this range, with current drive efficiencies ranging from 32 to 45 kA/MW. The current drive arises from the Ohkawa effect[17], rather than the conventional Fisch-Boozer effect, and therefore is driven opposite to the direction of the launched waves. The large trapped particle fraction on the low field side of the plasma at low aspect ratio leads to the high current drive efficiency The heating and CD deposition results from GENRAY/CQL3D are used in the simulations, and further details can be found for NSTX in ref[9].

Two cases are identified from the simulations for the high β 100% non-inductive regime, one with I_P = 800 kA and the NB driven current density and power deposition from TRANSP analysis of 109070, and one at 1.0 MA utilizing an arbitrary broadening of the power deposition and current density profile. The lower current case requires 10% higher energy confinement than 109070, has an on axis density of $n_{20}(0) = 0.44$, $\beta_N = 8.2$ and $\beta = 31\%$. The central safety factor drops to 1.2 and remains there. There is 433 kA of bootstrap current, 227 kA of NB driven current, and 105 kA of EBW current, with the non-inductive current fraction equal to 100%. The higher current case requires 25% higher energy confinement than 109070, has an on axis density of $n_{20}(0) = 0.42$, $\beta_N = 8.9$, and $\beta = 42\%$. The central safety factor drops to 1.7 and remains there. There is 461 kA of bootstrap current, 390 kA of NB driven current, and 100 kA of EBW current, with the non-inductive current fraction equal to 100%. Shown in Fig. 11 are the time evolutions of the central safety factors and the parallel current densities for the two projected plasmas. The broadening of the NB driven current profile in the higher β case allowed access to higher plasma current without forcing the central safety factor too low. In order to examine this possibility on the experiment, efforts to characterize the NB driven current profile under various high and low frequency MHD, high and low toroidal field, as well other operating conditions are underway. An interesting alternative is provided by the recent long pulse experiments (116313) that obtain strong density peaking, high density, and higher bootstrap

current, which could serve the same purpose of displacing more of the non-inductive current off-axis.

The current redistribution times for these plasmas are 0.5 to 0.7 s, yielding roughly 4-6 current relaxation times within the plasma current flattop. Both these plasmas are stable to $n = \infty$ ballooning modes and n = 1 and 2 external kink modes with a wall approximately at the NSTX structure locations. The structure models used for the low-n stability are shown in Fig. 1. Since these plasmas exceed the no-wall β limit they will require resistive wall mode stabilization from the plasma rotation and/or feedback coils. The long pulse experimental plasmas described in Section III already exceed the no-wall β limit and are sustained by plasma rotation. Analysis indicates that simultaneous high κ and δ, off-axis CD from EBWs, elevated q(0) above 1.0, and RWM stabilization are critical to accessing this stable high β regime.

VII. Simulations of Non-solenoidal Current Rampup

The non-solenoidal initiation and current rampup is a critical goal of the ST program since its attractiveness is directly tied to eliminating the OH central solenoid on the inboard side of the device and allowing access to compact geometry. A discharge to achieve this goal can be divided into three phases; the breakdown and startup with Coaxial Helicity Injection (CHI) or the outer poloidal field coils (described elsewhere[18,19]), the early plasma current rampup and heating with High Harmonic Fast Waves (HHFW), and the later plasma current rampup and heating from both HHFW and NBI. The first phase is not modeled here and will not be discussed further in this study. The time scales required for non-inductive current rampup are long compared to those required with inductive current rampup, since the inductive ramp rate is limited by the current redistribution time at the plasma edge while the non-inductive current ramp rate is limited by the current redistribution time at the plasma center[20]. It is possible to form a "current hole" during strong non-inductive current rampup, however, the drive for this is the time dependent increase in off-axis non-inductive current, which cannot be sustained indefinitely. For the present simulations current holes are avoided, since they can not presently be treated in the TSC. The available flattop is determined by the TF coil, ranging from 1.5 s at 0.5 T to 5.0 s at 0.3 T.

Virtually no experimental information is available for this type of discharge on NSTX, so that simulations must rely on reasonable assumptions and theoretical models. These assumptions are being examined critically based on experimental results as they become available. The simulations assume that the plasma starts the non-inductive rampup at I_P = 100 kA, provided by the initiation phase, which is treated in the code as inductive current. HHFW is the heating and current drive source in this low I_P and low T_e phase, and NBI is added in the higher I_P phase when the I_P rate of increase is slowing down. The toroidal field is 0.45 T allowing a maximum of 1.8 s of pulse length. In the low I_P phase the HHFW power is ramped slowly to avoid current hole formation, while the density is ramped to keep the temperature sufficiently low to access short core current redistribution time scales. In order to keep the temperature from increasing too fast in this phase the plasma is limited on the inboard wall to avoid transition to H-mode. The peak electron temperature reaches 1.3 keV, while the density ramps up to 0.3×10^{20} m^{-3} over 0.3 s. Around 0.3-0.4 s the plasma is diverted, allowing an improvement in global confinement. Then beginning at 0.5 s the 6 MW of NBI power is injected in steps, accounting for the poor beam fast ion confinement at these lower plasma currents. The NB power absorbed and subsequent driven current is based on the beam confinement observed in the I_P rampup in discharge 109070 from TRANSP. The heating and driven current from the beam continue to improve as the plasma current increases, but the slow current rise keeps the absorbed power low in these simulations, only reaching 2-3 MW for 6 MW of injected power. The poloidal β_P reaches 2.8, β_N reaches about 5.0, li(1) drops to 0.47, and the central safety factor remains above 4.0 during the discharge simulation. The bootstrap current reaches 300 kA, and the HHFW driven current maximizes at 150 kA in the early phase and decreases when the density rises and NB fast ions are present to absorb HHFW power (calculated by CURRAY). The HHFW phasing is 7 m^{-1} co-CD (same direction as the plasma current) and up to 6 MW are injected. By 1.8 s the total plasma current has reached just over 420 kA. Since the beam ions are not well confined, at these low plasma currents a significant HHFW current persists, in spite of parasitic absorption of HHFW power on fast NB ions. These results are shown in Fig. 12 giving the contributions to the plasma current, density and electron and ion peak temperatures as a function of time. Another simulation of the non-solenoidal rampup was done at the lower toroidal field of 0.35 T, which would allow 3.4 s of flattop. This simulation showed similar behavior to the 0.45 T case, although by 3.4 s the plasma current reached 480 kA, β_N reached 6.2, and the central safety

factor drops to 2.0. The higher β_N value at reduced toroidal field indicates that RWM stabilization may be required, however, the weaker NB absorption at low current will tend to reduce the beam driven rotation. It appears that NSTX does not have sufficient pulse length to reach a plasma current of at least 800 kA to connect to a high performance plasma configuration, but can demonstrate the critical features of the non-inductive rampup.

Experiments have begun to examine the HHFW heating and current drive at low I_P. Shown in Fig. 13 is a segment of a discharge where the plasma current was ramped up and maintained at 250 kA with the solenoid. Up to 2.8 MW of HHFW power was injected with $k_{||} = 14$ m^{-1} heating phasing in an effort to drive the surface voltage to 0. The injection of power drives the stored energy up significantly and creates an H-mode confinement regime. The surface voltage is reduced to 0 or even slightly below, and the solenoid current becomes slightly inverted or flat indicating it is no longer providing volt-seconds to the plasma. Also shown in the figure are the electron temperature and density profiles at 4 time slices indicated on the time history plots. The starting profile shows the peak electron temperature of about 500 eV, which rises to 1.0 keV over the next 0.015 s from HHFW heating. This continues with the peak temperature reaching 1.5 keV and an H-mode temperature pedestal beginning to form 0.040 s later. Finally after 0.10 s the electron temperature profile has broadened significantly generating high pedestal temperatures, and a lower peak temperature. This particular type of profile is ideal since it will generate a large bootstrap current, but keep the central temperature low enough to allow a reasonable I_P ramp rate. Unfortunately the HHFW power was driven to zero by feedback on the measured voltage across the antenna straps, and future efforts will concentrate on avoiding this to establish more stationary conditions.

Other experiments were done to examine whether the HHFW could sustain the plasma current if the solenoid current was clamped, stopping it from providing volt-seconds to the plasma. Shown in Fig. 14 are the results of one of these discharges. Here the solenoid is used to ramp the plasma current up to 300 kA, and then the solenoid current is clamped at 0.25 s. The plasma current will decay if no heating or CD is provided. When HHFW, with $k_{||} = 7$ m^{-1} co-CD phasing, is applied the plasma enters an H-mode, and following the solenoid current clamp, slows the plasma current decay. In this case the plasma later transitioned out of the H-mode and the current decay resumed similar to the no HHFW case. Also shown in the figure are the pressure profiles for the

case without and with HHFW, showing the significantly higher stored energy with HHFW, which will drive bootstrap current. How much current was driven by the HHFW needs to be better understood, and will require performing co-CD and counter-CD experiments at a range of power levels.

The modeling used for the non-solenoidal simulations raises several questions that require experimental verification. The plasma current and electron temperature provided by CHI or outer PF coil startup is unclear at this point, so experiments will continue to reduce the plasma current at which HHFW is injected. In addition, the plasma must be close to the antenna for good power coupling, and experimental proposals for positioning the plasma on the antenna limiter at early times are being developed. The HHFW heating and driven current are determined by ray-tracing calculations with CURRAY, however, experiments show that there can be parasitic absorption mechanisms that reduce the power that reaches the plasma core (and subsequently reduce the CD) as a function of the antenna phasing. For example, the calculations indicate that the lowest $k_{||}$ phasings have the highest CD efficiencies, while experiments show that the highest $k_{||}$ phasings have the largest increase in peak electron temperature per unit power. This observation along with other diagnostic results point toward mechanisms that reduce the power reaching the plasma core. Experiments have already begun to identify these trends in the low I_P regime. The energy confinement assumptions in the simulations were based on higher I_P HHFW experiments, but the recent experiments described above indicate that H-mode is required for the HHFW to replace the inductively driven plasma current, and these experiments will continue particularly to determine how to sustain the HHFW H-mode. The later phase of the non-inductive current rampup involves injecting NBs, but at low plasma currents where the absorption is much weaker than typical discharges in NSTX. A dedicated effort to characterize the NB capability at low I_P will be proposed for the next run period. As part of this, the compatibility of simultaneous HHFW and NBI in the low I_P regime will need to be assessed.

VIII. Conclusions

There has been substantial progress on producing long pulse plasmas in NSTX. The discharge pulse length has reached the I^2t heating limit for the toroidal field coil giving multiple current relaxation times for the sustainment of the plasma current, high β_N, and current profile. Plasma elongations are routinely above 2.25, the high β_N phase is above the no-wall n=1 limit, and non-

inductive current fractions are exceeding 70%. Considerable evolution has occurred over the last 3 run campaigns (2002, 2004, 2005) toward these plasmas, and the differences between the discharges are being examined to understand how to optimize this operating regime.

Simulations of advanced ST plasma scenarios for NSTX using TSC have shown that the 100% non-inductive current, and 100% non-inductive high β objectives may be achieved, based on reasonable extrapolations of existing experimental discharges. The 100% non-inductive scenarios, based on the discharge 109070 (2002), with NBI heating/CD achieve bootstrap current fractions of 45% at I_P = 800 kA, require energy confinement already achieved on NSTX, and reach β_N and β values of 4.7 and 13%, respectively. This is accomplished by increasing the plasma elongation from 2.0 to 2.5, utilizing an early heating/H-mode transition to elevate the central safety factor, and reducing the density to enhance the NB driven current. Simulations based on the most recent long pulse discharges 116313 (2005) show a significantly different energy confinement regime from 109070, that may be produced by the differences between the NB power absorption at the H-mode transition, affecting how the safety factor evolves. Since the discharge 116313 has incorporated higher κ and an early heating/H-mode approach, simulations were done to project this discharge to lower density operation in order to reach 100% non-inductive current, showing that this does increase NB current drive, but must be balanced against producing peaked current profiles which drive the central safety factor to 1.0.

The 100% non-inductive high-β scenarios at lower B_T with NBI and EBW off-axis current drive achieve bootstrap current fractions of 45-50% at I_P = 0.8-1.0 MA, require energy confinement 10-25% higher than achieved on NSTX, and reach β_N and β_T values of 8.2-8.9 and 31-43%, respectively. Broadening of the NB driven current profile was found to allow access to the I_P = 1.0 MA with $\beta \approx 40\%$ regime, and characterization of the current density profile on high and low frequency MHD, B_T, and other plasma parameters in the experiment is being done.

The non-solenoidal current rampup simulations show that NSTX can address the critical features of this approach, addressing many of the challenges for future ST devices without a solenoid. The HHFW current drive is a critical feature of the low I_P ramp phase to connect the early startup to the NBI heating and CD phase. NSTX's pulse lengths are probably not sufficient to provide non-solenoidal rampup to a high performance plasma at I_P = 800 kA or higher. Experiments to

address the HHFW heating/CD phase have begun, showing early signs of replacing the solenoid in I_P = 250-300 kA regime. In addition, sustaining an H-mode in these experiments appears a necessary feature to achieve this. The numerous assumptions made in the simulations of the non-solenoidal current rampup are being critically examined to formulate experiments for their verification, which is already leading to improved simulations.

Integrated simulations of NSTX to reproduce experimental discharges, and then project to regimes not yet produced in the experiment provides a means to focus experiments on the most critical features to access the advanced ST plasmas and establish their physics basis for future devices. The feedback of experimental data to update and improve the simulations is critical to progressively reduce the level of extrapolation.

Acknowledgements

Work supported by US DoE contract DE-AC02-76CH03073

References

[1] M. Ono, M. Peng, C. E. Kessel, *et al*., Nucl. Fusion **44**, 452 (2004).

[2]] ITER Physics Basis, Nuc. Fusion **39**, 2175 (1999).

[3] S. C. Jardin, N. Pomphrey, and J. DeLucia, J. Comp. Phys. **66**, 481 (1983).

[4] R. Budny, M. G. Bell, H. Biglari, *et al*., Nucl. Fusion **32**, 429 (1992).

[5] R.J. Goldston D. C. McCune, H. H. Towner, S. L. Davis, R. J. Hawryluk, and G. L. Schmidt, J. Comp. Phys. **43**, 61 (1981).

[6] A. Pankin, D. McCune, R. Andre, G. Bateman, and A. Kritz, Comp. Phys. Comm. **159**, 157 (2004).

[7] T.K. Mau, S.C. Chiu, "RF Current Drive Modeling for Spherical Torus," Proc. 12th Top. Conf. on Radio Frequency Power in Plasmas, Savannah, AIP Conf. Proc. 403, 243 (1997).

[8] R.W. Harvey and M.G. McCoy, Proceedings of the IAEA Technical Committee on Advances in Simulation and Modeling of Thermonuclear Plasmas, Montreal, Quebec (International Atomic Energy Agency, Vienna, 1993), p. 489; USDOC NTIS Doc. No. DE93002962.

[9] G. Taylor, P. Efthimion, C. E. Kessel, R. W. Harvey, A. P. Smirnov, N. M. Ershov, M. D. Carter, and C. B. Forest, Phys. Plasmas **11**, 4733 (2004).

[10] J. DeLucia, S. C. Jardin, A. M. M. Todd, J. Comp. Phys. **37**, 183 (1980).

[11] J. M. Greene and M. S. Chance, Nucl. Fusion **21**, 453 (1981).

[12] R. C. Grimm, R. L. Dewar, and J. Manickam, J. Comp. Phys. **49**, 94 (1983).

[13] A. Glasser and M. Chance, Bull. Am. Phys. Soc. **42**, 1848 (1997).

[14] J. Bialek, A. H. Boozer, M. E. Mauel, and G. A. Navratril, Phys. Plasmas **8**, 2170 (2001).

[15] J. E. Menard, M. G. Bell, E. E. Bell, *et al.*, Nuc. Fusion **43**, 330 (2003).

[16] C. E. Kessel, A. Garofalo, and T. Terpstra, "Simulation of DIII-D Flat q Discharges", 31st European Physical Society Conference on Plasma Physics, London, (2004), Europhysics Conference Abstracts Vol. 28G (2004); http://eps2004.clf.rl.ac.uk/pdf/P2-186.pdf.

[17] T. Ohkawa, General Atomics Report #4356.007.001 (1976).

[18] R. Raman, T. R. Jarboe, R. G. O'Neill, W. T. Hamp, B. A. Nelson, V. A. Izzo, A. J. Redd, P. E. Sieck, and R. J. Smith, Nuc. Fusion **45**, L15 (2005).

[19] M. Ono, M. G. Bell, R. E. Bell, *et al.*, Plas. Phys. Cont. Fus. **45**, 657 (2003).

[20] S. C. Jardin, Nucl. Fusion **40**, 1101 (2000).

Figure Captions

Figure 1. (color) The 1.0 MA high β plasma cross-section is shown with two wall models used in the low-n stability analysis, the closer wall lies on actual conducting structure locations in NSTX, while the other is a more conservative wall to approximate the nonaxisymmetric nature of the conducting structures.

Figure 2. (color) Experimental time traces of the plasma current and NB injected power (a), and plasma elongation and internal self-inductance (b) for discharges 109070 (2002, black), 112546 (2004, red), and 116313 (2005, green). Plasma elongation and internal self-inductance have suppressed zeros to clarify the differences between discharges during the flattop phases.

Figure 3. (color) Experimental time traces of the peak electron density (a), surface voltage (b), peak electron temperature (c), and normalized β (d) for discharges 109070 (2002, black), 112546 (2004, red), and 116313 (2005, green). The onset of MHD reducing the stored energy is noted.

Figure 4. (color) Time history of the peak electron and ion temperatures (a) from the TSC simulation of the discharge 109070, and the data from Thomson scattering and Charge Recombination Spectroscopy diagnostics. The profiles for the safety factor, ion and electron thermal diffusivities, ion and electron temperatures, and density at the time 0.45 s (b). The total parallel current density, with bootstrap and NBI contributions at 0.45 s (c).

Figure 5. (color) Time history of the plasma current and total non-inductive current (a), and central safety factor (b) for the simulation of discharge 109070 (pink) and the projected discharge using high κ, density control, and early heating/H-mode (blue). The minimum value of the ordinate axis for the safety factor is 0.5. The total parallel current densities (solid) for 109070 (pink) and the projected discharge (blue), with bootstrap (dotted) and NBI (dashed) contributions at 0.45 s and 1.45 s, respectively (c).

Figure 6. (color) Time history of the peak electron and ion temperatures from the TSC simulation of the discharge 116313 and the data from Thomson scattering and Charge Recombination Spectroscopy diagnostics (a). Time history of the peak, line average, and volume average electron densities for discharge 116313 (b). The profiles for the safety factor, ion and electron thermal diffusivities, ion and electron temperatures, and density at the time 0.98 s (c). The total parallel current density (black), with bootstrap (red) and NB (blue contributions at 0.98 s (d).

Figure 7. (color) Time histories of the contributions to the plasma current from bootstrap (red), NBCD (blue), and diamagnetic and Phirsch-Schluter currents (pink) (a), and the central safety factor (b) from the simulation of the discharge 116313 and the MSE constrained EFIT equilibrium reconstructions. The minimum value of the ordinate axis for the safety factor is 0.5.

Figure 8. (color) The safety factor profiles versus time from the simulations of discharges 109070 (a) and 116313 (b) showing the presence of reversed shear generated after 0.2 s in 109070 with the discharge lasting until 0.55 s, and the early loss of reversed shear by 0.15s in 116313 with the discharge lasting until 1.5 s. This may be responsible for the strongly different confinement regimes. The minimum value of the ordinate axis for the safety factor is 0.5.

Figure 9. (color) Time histories of the central safety factors for projected discharges based on 116313 (a) at lower density $n_{20}(0) = 0.42$, for peaked ($n(0)/\langle n\rangle = 1.7$) and broad density($n(0)/\langle n\rangle = 1.15$) at high and low energy confinement. The central safety factor reaching 1.0 is indicated by the circles for each case. The minimum value of the ordinate axis for the safety factor is 0.5. The total parallel current density (black) and NBCD contributions (blue) for the reference discharge 116313 simulation (dashed) and the projected low density case (solid) with the highest non-inductive current (b), which has peaked density and $H_{98} = 1.2$.

Figure 10. (color) Profiles of the current density deposited by Electron Bernstein Wave current drive from calculations with GENRAY/CQL3D with frequencies of 14 and 28 GHz and plasma $\beta = 20$ and 40%, for NSTX, showing similar deposition locations and total driven currents.

Figure 11. (color) Time histories of the central safety factors for the high β 100% non-inductive projected plasmas (a), based on discharge 109070, for 800 kA (solid) and 1.0 MA (dashed). The minimum value of the ordinate axis for the safety factor is 0.5. The parallel current densities (b) for the 800 kA (upper) and 1.0 MA (lower) cases, showing the total (black), bootstrap (red), NBCD (blue) and EBWCD (green) contributions. Indicated by the arrows is the NBCD width at half-maximum, the upper case using the discharge 109070 NBCD profile width, and the lower case using an assumed broader profile.

Figure 12. (color) Time histories of the plasma current (black), the total non-inductive current (yellow), and the contributions to the plasma current from bootstrap (red), HHFW CD (green), and NBCD (blue) (a).The peak electron and ion temperatures, and electron density (b) for the non-solenoidal I_P rampup simulation for NSTX at B_T = 0.45 s.

Figure 13. (color) Experimental time traces of the stored energy, surface voltage, injected HHFW power, and solenoid current (a) during a segment of the discharge 117605. The electron temperature and density profiles as function of major radius (b) at the time slices indicated on the time traces, 0.385 (green), 0.400 (yellow), 0.425 (blue), and 0.485 s (pink).

Figure 14. (color) Experimental time traces for the plasma current, stored energy, and injected HHFW power (a) for a discharge with HHFW 116449 and one without HHFW 116461, showing the slowing of the current decay while the plasma is in an HHFW H-mode.. The electron pressure profiles (b) for the two discharges at 0.285 s are also shown. The time of the OH coil current clamp is indicated by the yellow line at 0.25 s.

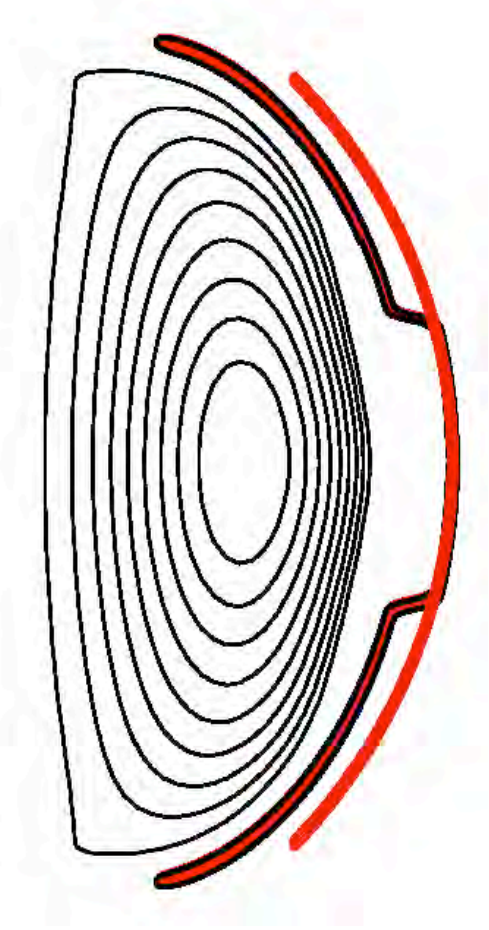

FIGURE 1

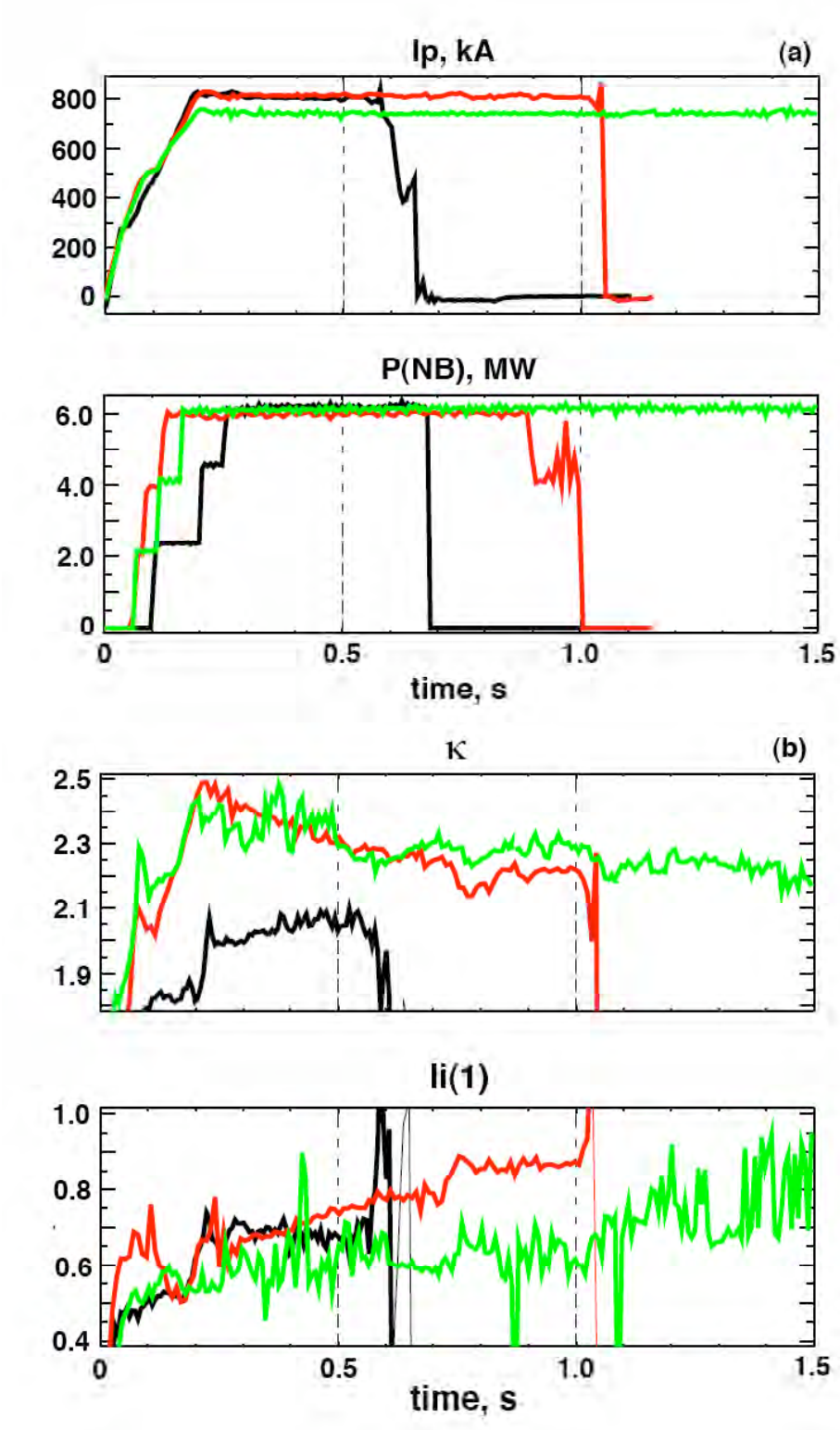
Ip, kA
(a)
800
600
400
200
0
P(NB), MW
6.0
4.0
2.0
0
0
0.5
1.0
1.5
time, s
κ
(b)
2.5
2.3
2.1
1.9
li(1)
1.0
0.8
0.6
0.4
0
0.5
1.0
1.5
time, s

FIGURE 2

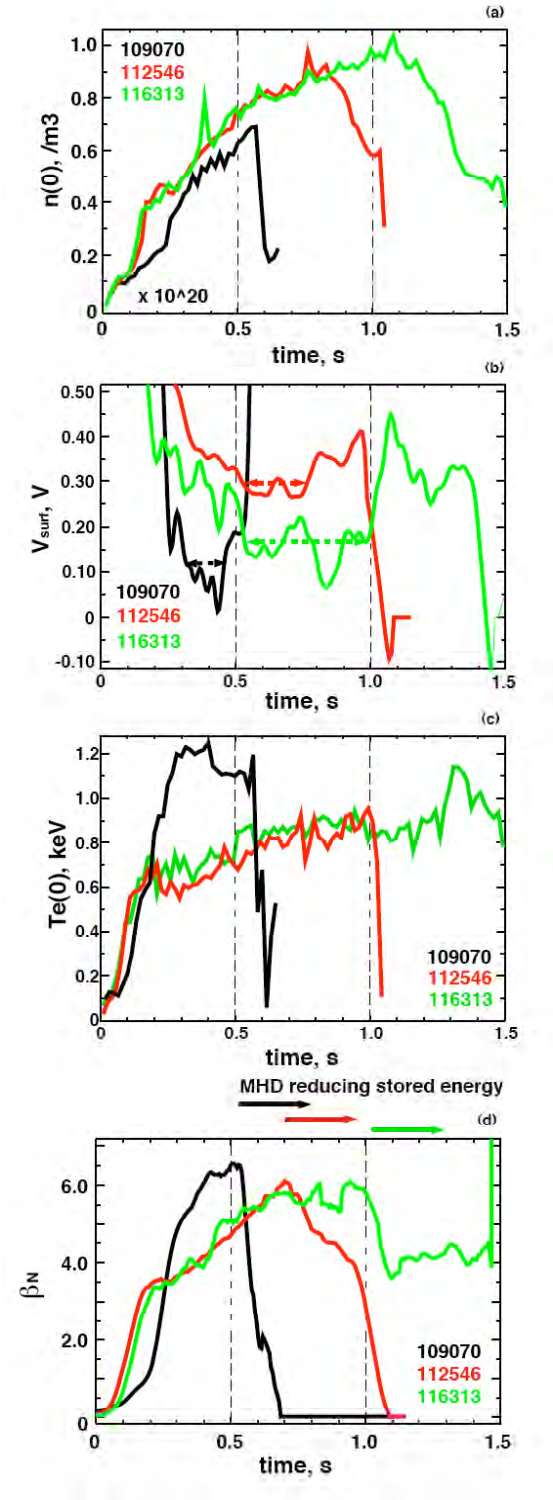
(a)
109070
112546
116313
n(0), /m3
x 10^20
time, s
(b)
V_{surf}, V
109070
112546
116313
time, s
(c)
Te(0), keV
109070
112546
116313
time, s
MHD reducing stored energy
(d)
β_N
109070
112546
116313
time, s

FIGURE 3

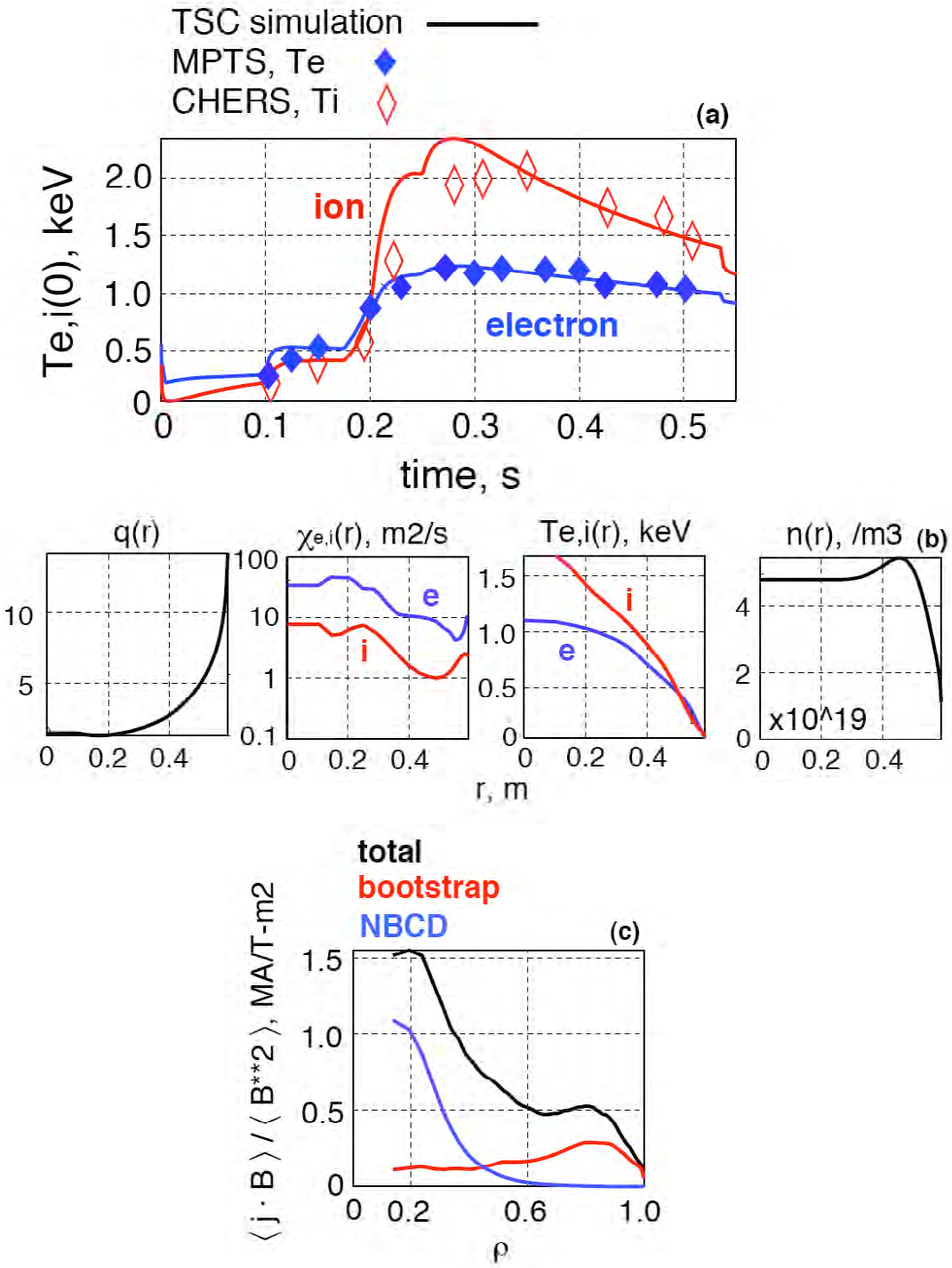
TSC simulation
MPTS, Te
CHERS, Ti
(a)
Te,i(0), keV
ion
electron
time, s
q(r)
χe,i(r), m2/s
e
i
Te,i(r), keV
n(r), /m3
(b)
x10^19
r, m
total
bootstrap
NBCD
(c)
⟨ j · B ⟩ / ⟨ B**2 ⟩, MA/T-m2
ρ

FIGURE 4

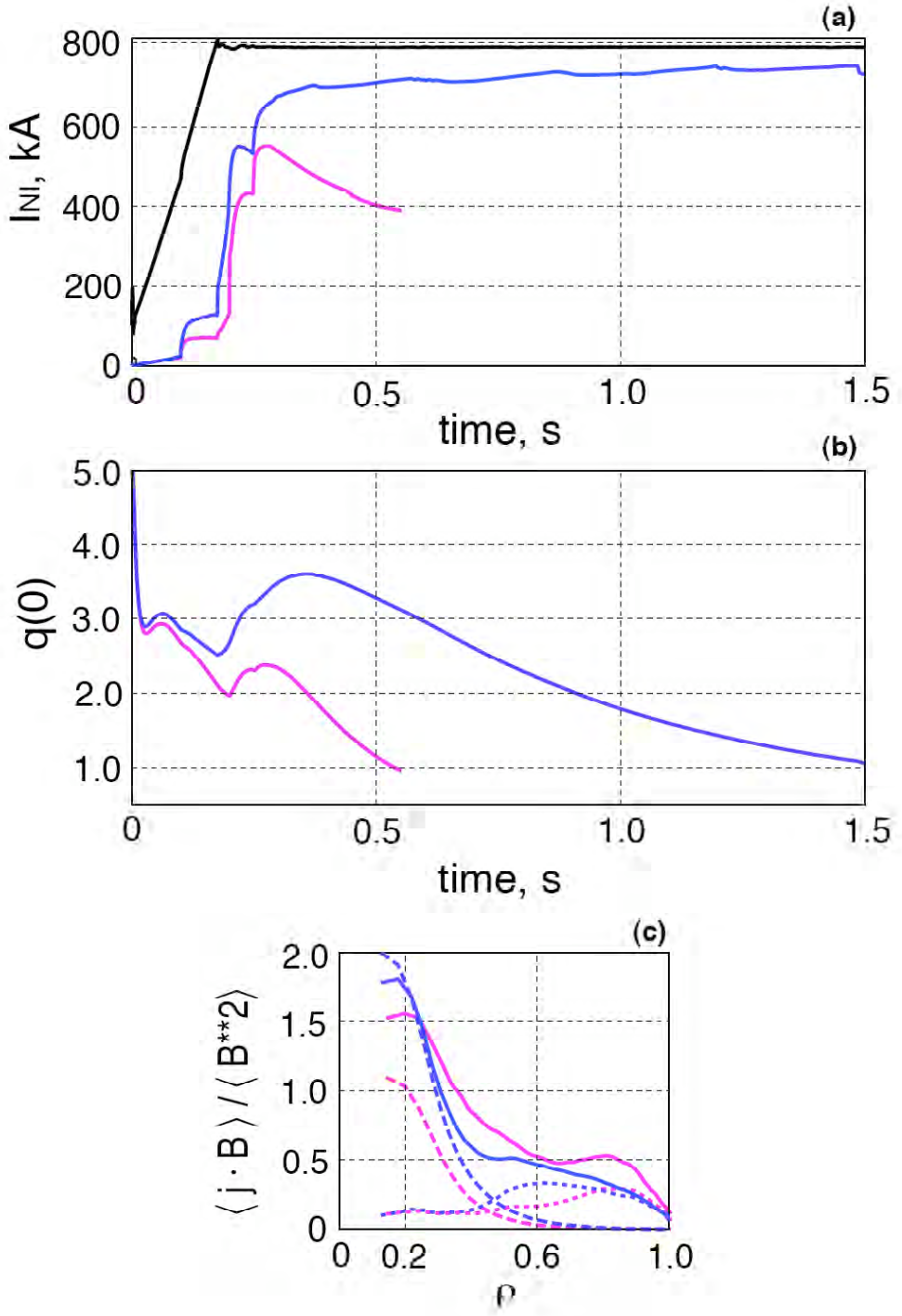
(a)
800
600
400
200
0
I_{NI}, kA
0
0.5
1.0
1.5
time, s
(b)
5.0
4.0
3.0
2.0
1.0
q(0)
0
0.5
1.0
1.5
time, s
(c)
2.0
1.5
1.0
0.5
0
⟨ j · B ⟩ / ⟨ B**2 ⟩
0
0.2
0.6
1.0
ρ

FIGURE 5

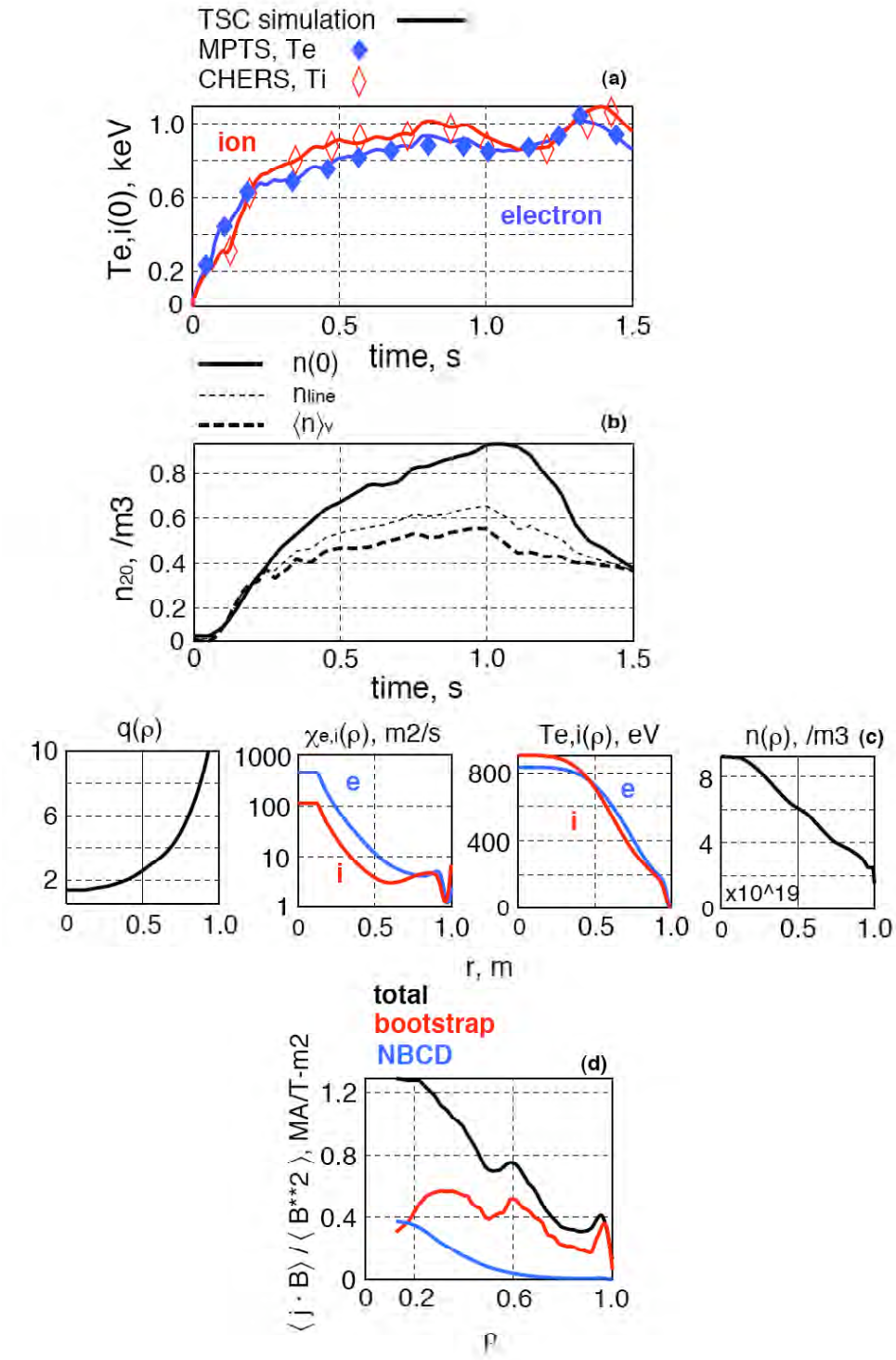
TSC simulation
MPTS, Te
CHERS, Ti
(a)
Te,i(0), keV
ion
electron
time, s
n(0)
nline
⟨n⟩v
(b)
n20, /m3
time, s
q(ρ)
χe,i(ρ), m2/s
e
i
Te,i(ρ), eV
e
i
n(ρ), /m3 (c)
x10^19
r, m
total
bootstrap
NBCD
(d)
⟨ j · B⟩ / ⟨ B**2 ⟩, MA/T-m2
ρ

FIGURE 6

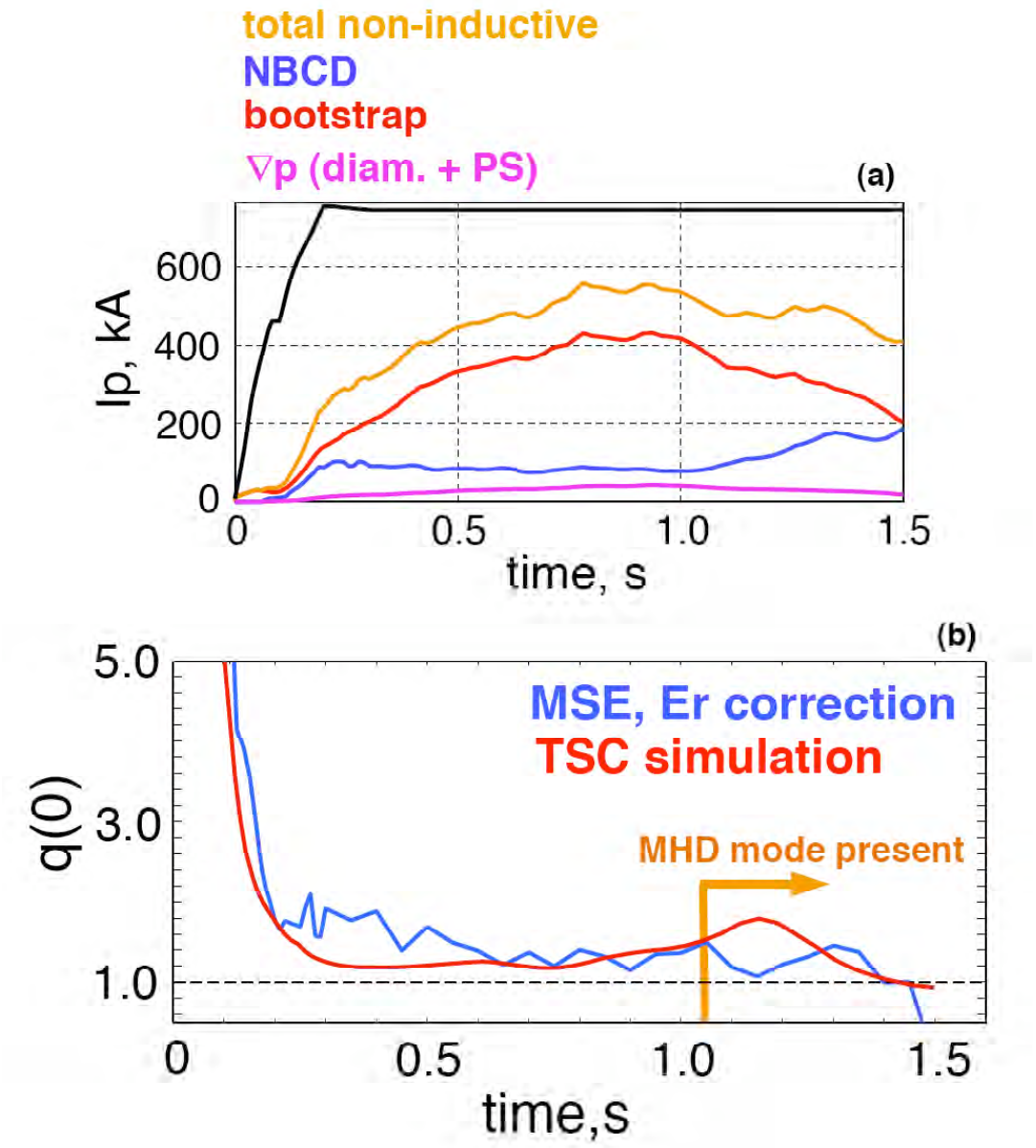
total non-inductive
NBCD
bootstrap
∇p (diam. + PS)
(a)
Ip, kA
600
400
200
0
0
0.5
1.0
1.5
time, s
(b)
5.0
3.0
1.0
q(0)
MSE, Er correction
TSC simulation
MHD mode present
0
0.5
1.0
1.5
time,s

FIGURE 7

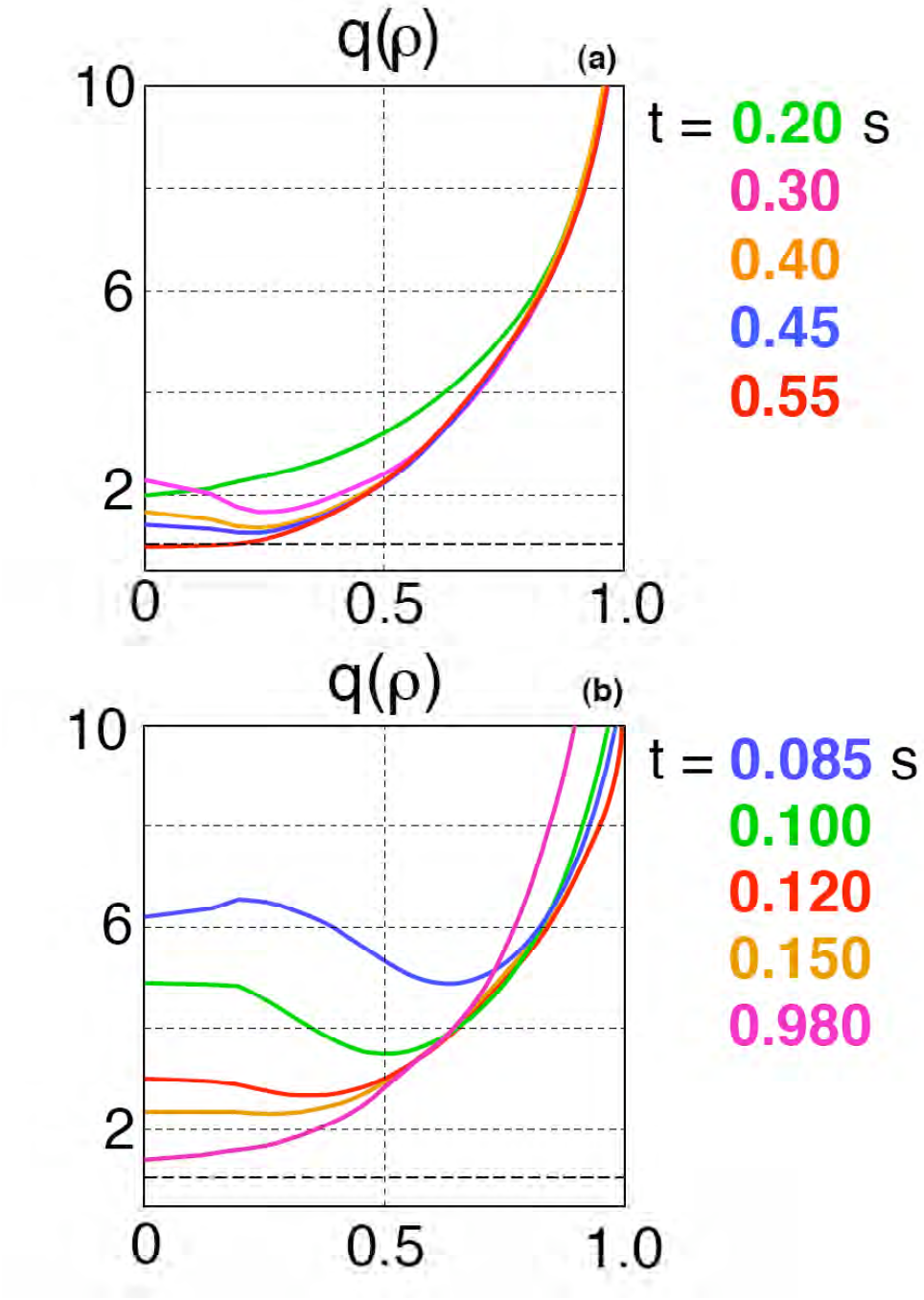
q(ρ)
(a)
10
6
2
0
0.5
1.0
t = 0.20 s
0.30
0.40
0.45
0.55
q(ρ)
(b)
10
6
2
0
0.5
1.0
t = 0.085 s
0.100
0.120
0.150
0.980

FIGURE 8

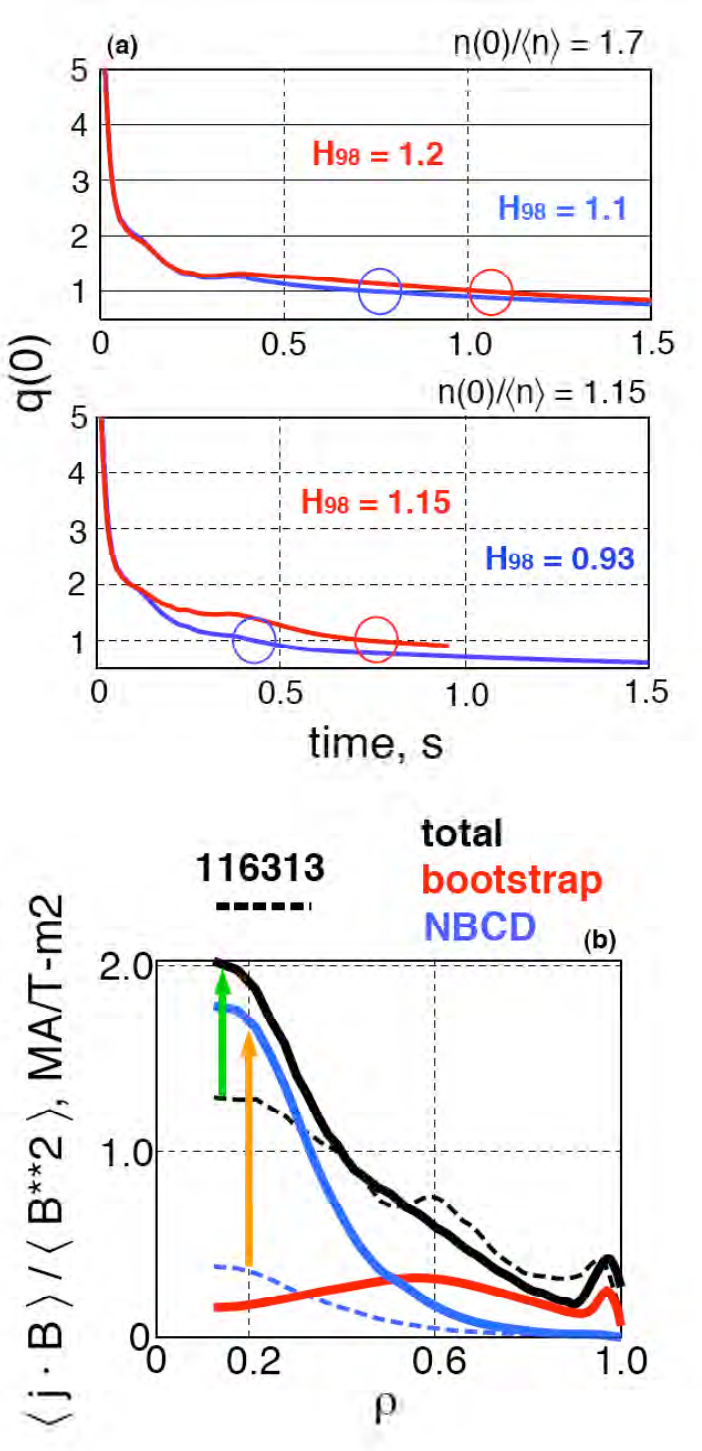
(a)
n(0)/⟨n⟩ = 1.7
H98 = 1.2
H98 = 1.1
q(0)
n(0)/⟨n⟩ = 1.15
H98 = 1.15
H98 = 0.93
time, s
116313
total
bootstrap
NBCD
(b)
⟨ j · B ⟩ / ⟨ B**2 ⟩, MA/T-m2
ρ

FIGURE 9

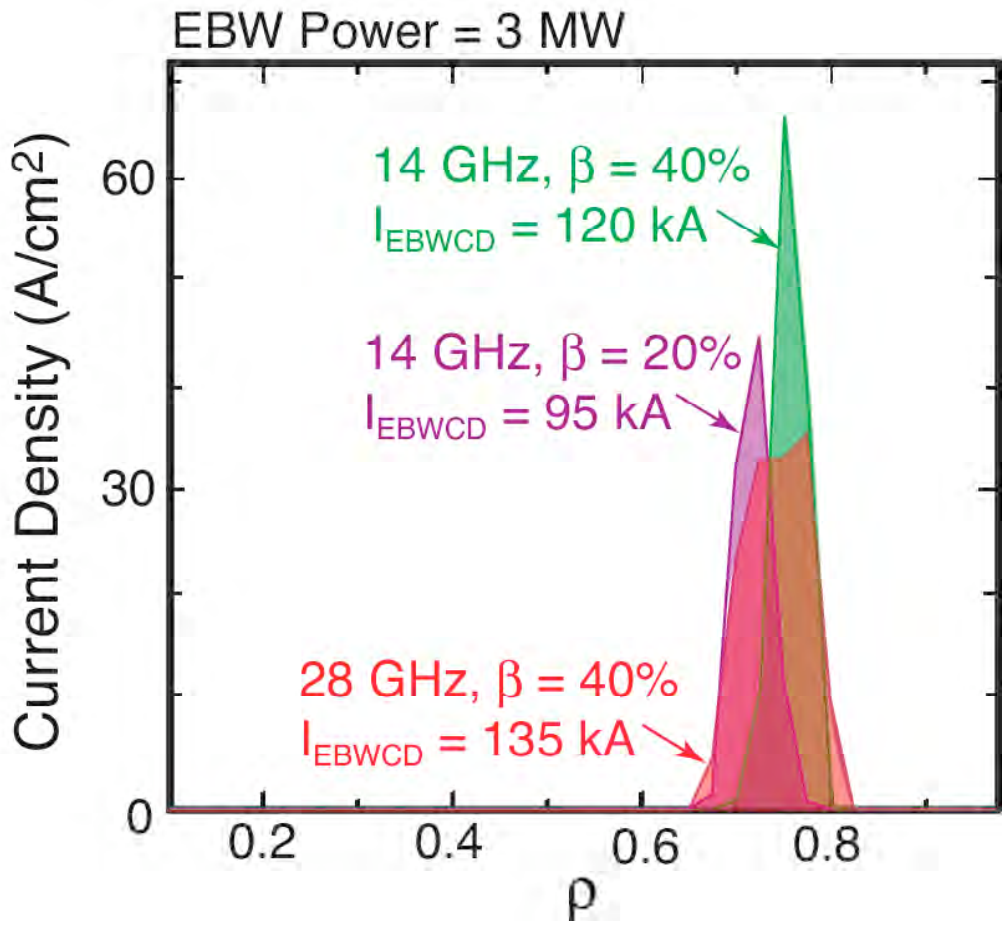
EBW Power = 3 MW
Current Density (A/cm²)
60
30
0
0.2
0.4
0.6
0.8
ρ
14 GHz, β = 40%
I_EBWCD = 120 kA
14 GHz, β = 20%
I_EBWCD = 95 kA
28 GHz, β = 40%
I_EBWCD = 135 kA

FIGURE 10

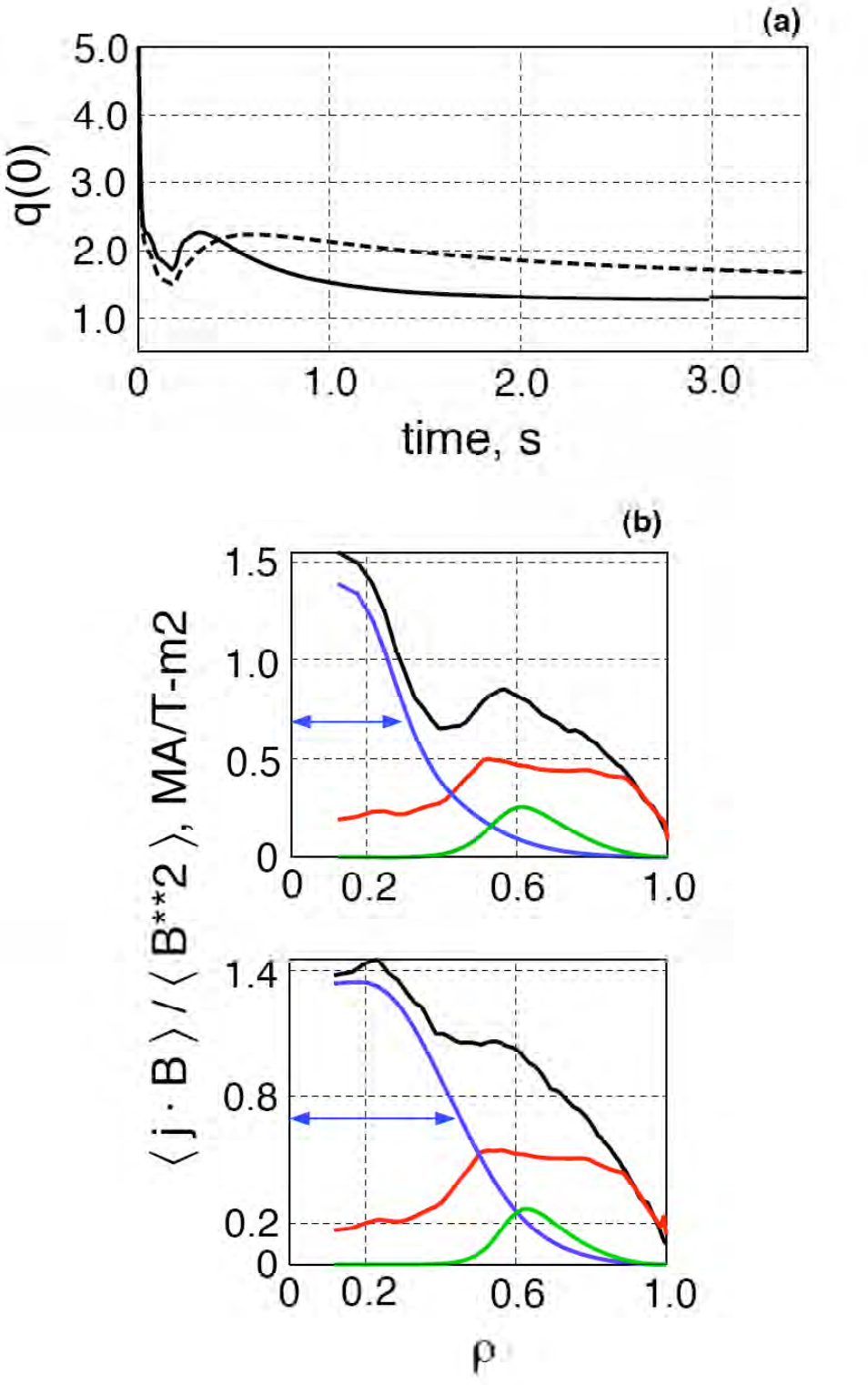
(a)
5.0
4.0
3.0
2.0
1.0
q(0)
0
1.0
2.0
3.0
time, s
(b)
1.5
1.0
0.5
0
0
0.2
0.6
1.0
1.4
0.8
0.2
0
0
0.2
0.6
1.0
ρ
⟨ j · B ⟩ / ⟨ B**2 ⟩, MA/T-m2

FIGURE 11

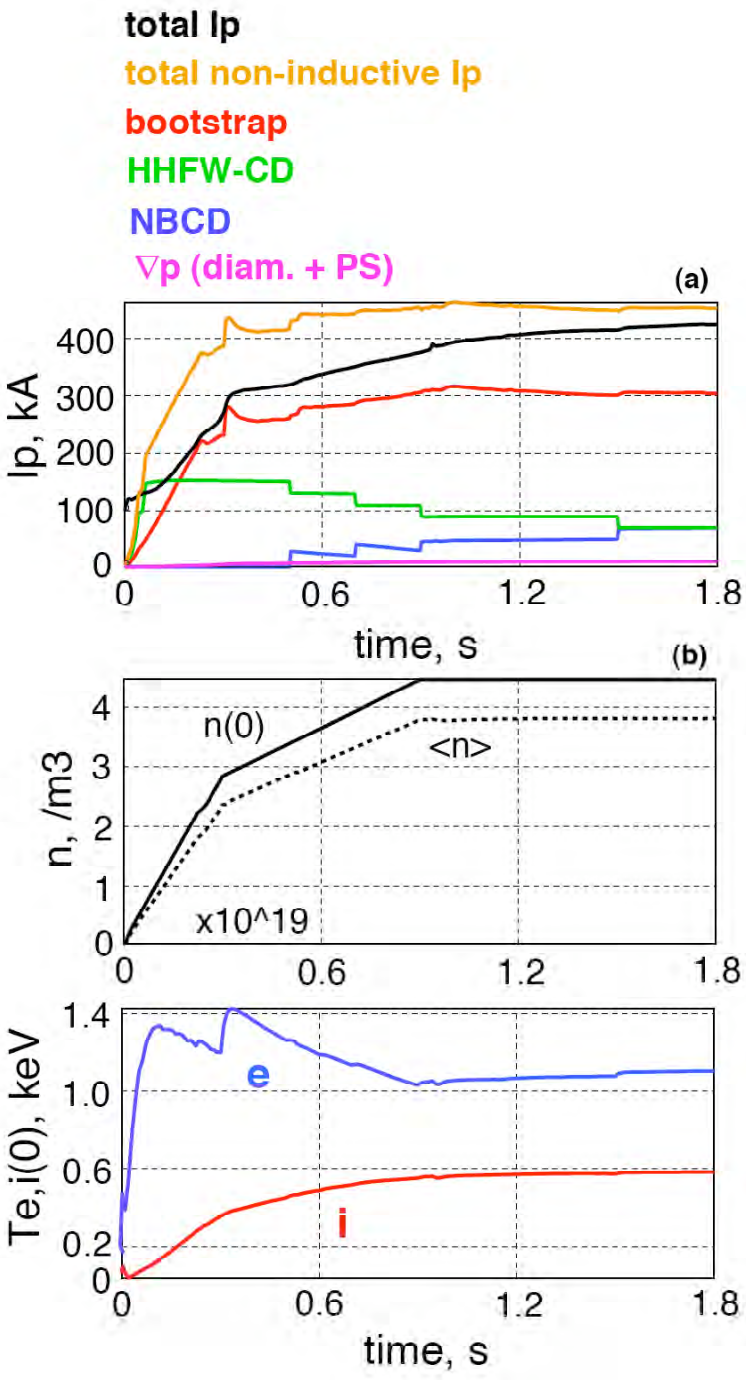
total Ip
total non-inductive Ip
bootstrap
HHFW-CD
NBCD
∇p (diam. + PS)
(a)
Ip, kA
400
300
200
100
0
0
0.6
1.2
1.8
time, s
(b)
n, /m3
4
3
2
1
0
n(0)
<n>
x10^19
0
0.6
1.2
1.8
Te,i(0), keV
1.4
1.0
0.6
0.2
0
e
i
0
0.6
1.2
1.8
time, s

FIGURE 12

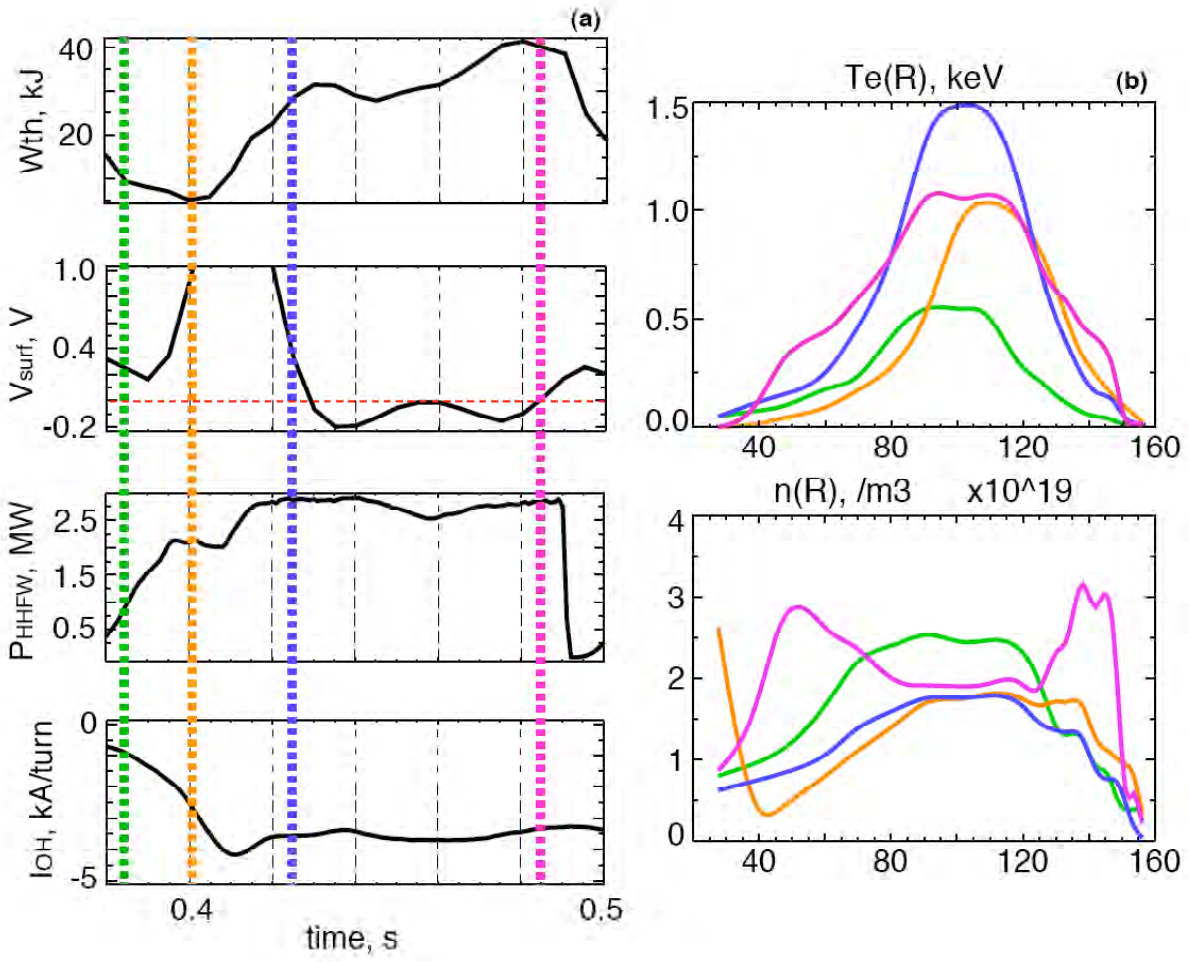
(a)
Wth, kJ
40
20
Vsurf, V
1.0
0.4
-0.2
PHHFW, MW
2.5
1.5
0.5
IOH, kA/turn
0
-5
0.4
0.5
time, s
Te(R), keV
(b)
1.5
1.0
0.5
0.0
40
80
120
160
n(R), /m3
x10^19
4
3
2
1
0
40
80
120
160

FIGURE 13

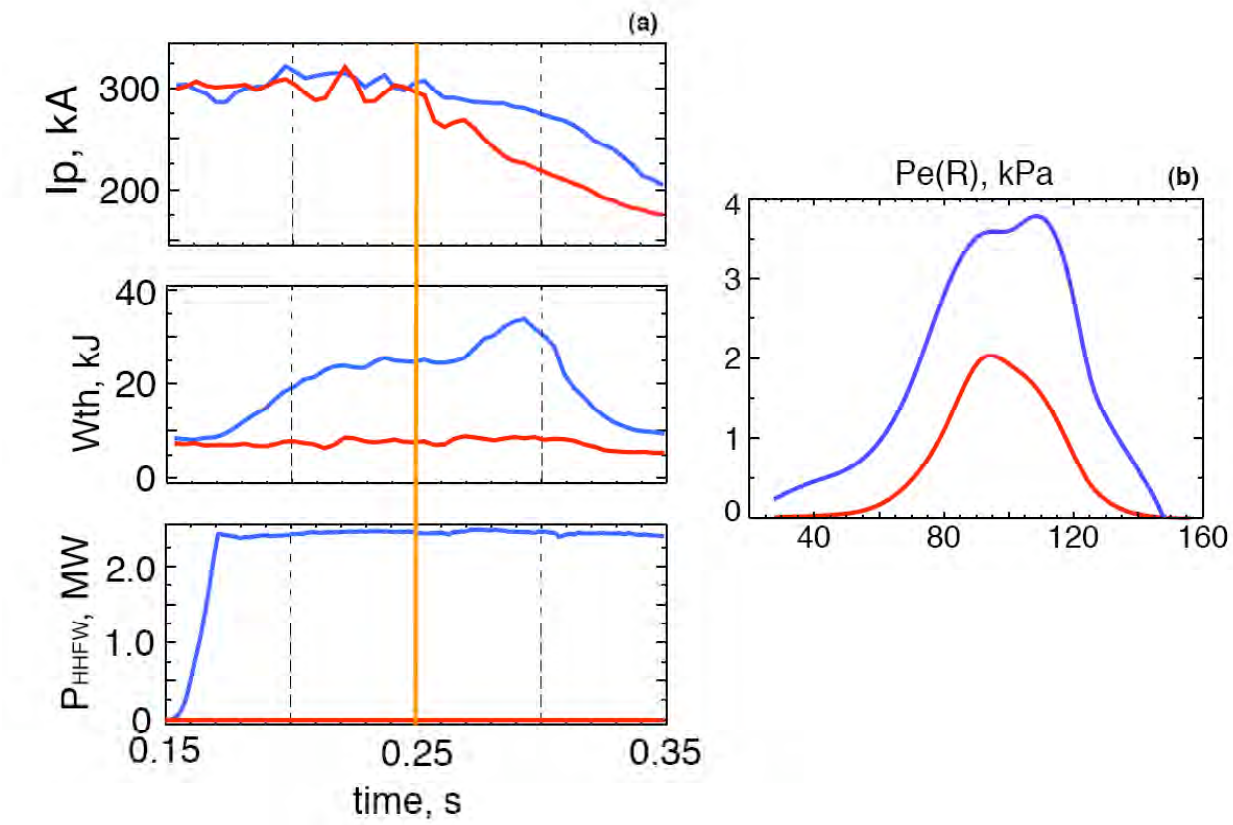
(a)
Ip, kA
300
200
Wth, kJ
40
20
0
P_HHFW, MW
2.0
1.0
0
0.15
0.25
0.35
time, s
Pe(R), kPa
(b)
4
3
2
1
0
40
80
120
160

FIGURE 14

External Distribution

Plasma Research Laboratory, Australian National University, Australia
Professor I.R. Jones, Flinders University, Australia
Professor João Canalle, Instituto de Fisica DEQ/IF - UERJ, Brazil
Mr. Gerson O. Ludwig, Instituto Nacional de Pesquisas, Brazil
Dr. P.H. Sakanaka, Instituto Fisica, Brazil
The Librarian, Culham Science Center, England
Mrs. S.A. Hutchinson, JET Library, England
Professor M.N. Bussac, Ecole Polytechnique, France
Librarian, Max-Planck-Institut für Plasmaphysik, Germany
Jolan Moldvai, Reports Library, Hungarian Academy of Sciences, Central Research Institute for Physics, Hungary
Dr. P. Kaw, Institute for Plasma Research, India
Ms. P.J. Pathak, Librarian, Institute for Plasma Research, India
Dr. Pandji Triadyaksa, Fakultas MIPA Universitas Diponegoro, Indonesia
Professor Sami Cuperman, Plasma Physics Group, Tel Aviv University, Israel
Ms. Clelia De Palo, Associazione EURATOM-ENEA, Italy
Dr. G. Grosso, Instituto di Fisica del Plasma, Italy
Librarian, Naka Fusion Research Establishment, JAERI, Japan
Library, Laboratory for Complex Energy Processes, Institute for Advanced Study, Kyoto University, Japan
Research Information Center, National Institute for Fusion Science, Japan
Professor Toshitaka Idehara, Director, Research Center for Development of Far-Infrared Region, Fukui University, Japan
Dr. O. Mitarai, Kyushu Tokai University, Japan
Mr. Adefila Olumide, Ilorin, Kwara State, Nigeria
Dr. Jiangang Li, Institute of Plasma Physics, Chinese Academy of Sciences, People's Republic of China
Professor Yuping Huo, School of Physical Science and Technology, People's Republic of China
Library, Academia Sinica, Institute of Plasma Physics, People's Republic of China
Librarian, Institute of Physics, Chinese Academy of Sciences, People's Republic of China
Dr. S. Mirnov, TRINITI, Troitsk, Russian Federation, Russia
Dr. V.S. Strelkov, Kurchatov Institute, Russian Federation, Russia
Kazi Firoz, UPJS, Kosice, Slovakia
Professor Peter Lukac, Katedra Fyziky Plazmy MFF UK, Mlynska dolina F-2, Komenskeho Univerzita, SK-842 15 Bratislava, Slovakia
Dr. G.S. Lee, Korea Basic Science Institute, South Korea
Dr. Rasulkhozha S. Sharafiddinov, Theoretical Physics Division, Insitute of Nuclear Physics, Uzbekistan
Institute for Plasma Research, University of Maryland, USA
Librarian, Fusion Energy Division, Oak Ridge National Laboratory, USA
Librarian, Institute of Fusion Studies, University of Texas, USA
Librarian, Magnetic Fusion Program, Lawrence Livermore National Laboratory, USA
Library, General Atomics, USA
Plasma Physics Group, Fusion Energy Research Program, University of California at San Diego, USA
Plasma Physics Library, Columbia University, USA
Alkesh Punjabi, Center for Fusion Research and Training, Hampton University, USA
Dr. W.M. Stacey, Fusion Research Center, Georgia Institute of Technology, USA
Director, Research Division, OFES, Washington, D.C. 20585-1290

The Princeton Plasma Physics Laboratory is operated
by Princeton University under contract
with the U.S. Department of Energy.

Information Services
Princeton Plasma Physics Laboratory
P.O. Box 451
Princeton, NJ 08543

Phone: 609-243-2750
Fax: 609-243-2751
e-mail: pppl_info@pppl.gov
Internet Address: http://www.pppl.gov